PROCEEDINGS OF SPIE

SPIEDigitalLibrary.org/conference-proceedings-of-spie

High-NA lensless coherent imager as a building block for a synthetic aperture interferometry array

Jorge Garcia-Armenta, Pablo D. Ruiz, Charles R. Coggrave, Ian S. Park, Jeremy Coupland

Jorge Garcia-Armenta, Pablo D. Ruiz, Charles R. Coggrave, Ian S. Park, Jeremy Coupland, "High-NA lensless coherent imager as a building block for a synthetic aperture interferometry array," Proc. SPIE 11056, Optical Measurement Systems for Industrial Inspection XI, 1105607 (21 June 2019); doi: 10.1117/12.2526153

SPIE.

Event: SPIE Optical Metrology, 2019, Munich, Germany

High-NA lensless coherent imager as a building block for a synthetic aperture interferometry array

Jorge Garcia-Armenta*, Pablo D. Ruiz, Charles R. Coggrave, Ian S. Park and Jeremy Coupland
Wolfson School of Mechanical, Electrical and Manufacturing Engineering, Loughborough University, Epinal Way, Loughborough, LE11 3TU, UK.

ABSTRACT

In digital holography, the field of view (FOV) and lateral resolution are limited by the pixel pitch and sensor dimensions, respectively. A large numerical aperture can be synthesized to increase the FOV and spatial resolution by coherently combining low resolution holograms obtained for different illumination and/or observation directions. This is known as Synthetic Aperture Interferometry (SAI) and in this work we describe the design, construction, calibration and testing of high numerical aperture compact coherent imagers (CI) which constitute the optical building block of a multi-sensor SAI array. The CIs consist of a photodetector array, a highly divergent reference beam close to it and an aperture that acts as a spatial filter to prevent aliasing of the digital holograms. We explore different optical designs to produce a highly divergent reference beam close to the sensor, including bulk optics, micro-optics, and ion beam milled optical fibres. An optimization approach is used to characterize the reference wavefront for accurate digital reconstructions of the scattered field first at the aperture plane and then at the object plane. The performance of a compact CI is demonstrated by reconstructing an object 76 mm wide at 80 mm from the sensor, which corresponds to a numerical aperture NA>0.5.

Keywords: Synthetic aperture interferometry, digital holography, numerical aperture, coherent imager, holographic camera.

1. INTRODUCTION

Coherent Scanning Interferometry (CSI) is considered by many as the gold standard for surface profilometry. It provides surface height maps with high axial and transverse resolution. Other powerful techniques for this purpose include focus variation microscopes, confocal microscopy and laser triangulation[1]. Inspection of large areas, e.g. thin film photovoltaic films with microscopic defects, can be performed by stitching together overlapping measurements. This is time consuming and usually an overkill, as defects constitute a very small fraction of the surface. A system capable of reconstructing the surface at the required resolution depending on the presence and size of defects would be able to accelerate these inspection tasks, e.g. by having the capability of locally adapting the spatial resolution in a large field.

Digital holography (DH) has been widely used as a phase evaluation method in microscopy[2], shape and surface measurements[3-4]. In DH, the FOV and lateral resolution are limited by the pixel pitch and sensor dimensions, respectively, but larger numerical apertures can be synthesized to increase both FOV and resolution by coherently adding low resolution holograms obtained for different illumination and/or observation directions. Known as synthetic aperture interferometry, this approach effectively increases the space-bandwidth product SBP (a measure of the amount of information that the optical system can capture, approximately the ratio between the area of the FOV and the central lobe of the point spread function)[5-6]. SAI is a well-established technique in the fields of radio astronomy and radar, and its most extreme achievement is perhaps the first image of a black hole[7]. In optical bandwidths, SAI has been implemented with different strategies to sample frequency space, e.g. by using a single receiver while varying the object's illumination angles[8], by fixing the illumination source while moving the sensor[9], by rotating the object[10] or by having a combination of multiple sources and receivers[11].

*J.Garcia@lboro.ac.uk

Optical Measurement Systems for Industrial Inspection XI, edited by Peter Lehmann, Wolfgang Osten, Armando Albertazzi Gonçalves Jr., Proc. of SPIE Vol. 11056, 1105607 · © 2019
SPIE · CCC code: 0277-786X/19/$21 · doi: 10.1117/12.2526153

An essential requirement in SAI is having a known phase relationship between each low-resolution hologram. Normally, a reference source placed next to the object under study serves as a common carrier to all combinations of illumination and observation directions (see Fig. 1) and separates the interference and autocorrelation terms in k-space. This solution, however, is not scalable and requires a reference source next to the object, which is not always feasible. An alternative approach consists of having independent coherent imagers (CI), i.e. phase-locked holographic cameras, each with its own reference source.

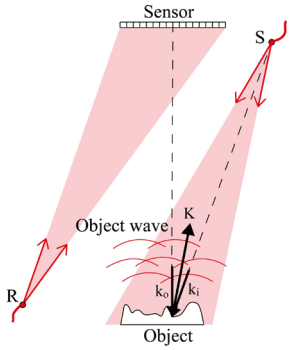

Figure 1. Fourier off-axis hologram with spatial carrier. The scattering vector is represented by K while k_i and k_o are the illumination and observation vectors respectively. S is the illumination source and R represents the reference source.

These could be arranged in large numbers in an array as the one shown is Fig. 2, which contains 225 of them. Also shown in Fig. 2, is a calibration plate used to determine the relative position between illumination sources and the apertures of the CIs. Each CI has a small aperture but is required to have a large FOV in order to synthesize a large aperture to reconstruct a large FOV at high resolution.

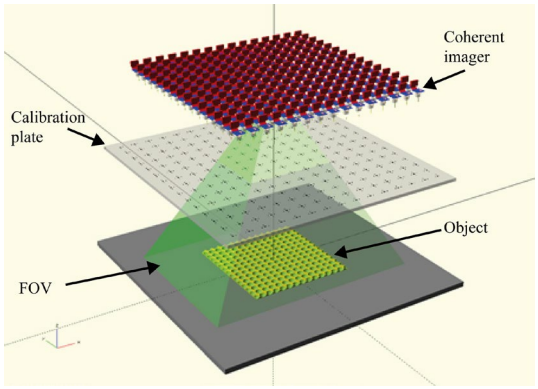

Figure 2. Schematic of an array of 15×15 CI's with a calibration plate to scan a surface.

In this paper, we describe the design and performance of lensless compact CIs with a high-NA, i.e. large FOV, as building blocks for a SAI array. Section 2 describes the basic design requirements of a compact CI, showing the evolution of the design towards a sensor as compact as possible.

In section 3 a method to characterize the reference wavefront is presented, which is a critical step towards a successful reconstruction of the object from the recorded holograms. Finally, in section 4 we demonstrate the performance of a compact CI with a large FOV, NA>0.5.

2. COHERENT IMAGER

2.1. Design considerations

The fundamental components of the CI as seen in Fig. 3 are a photodetector array (CMOS Sony IMX219 3.67 × 2.76 mm^2 colour sensor, 3280 × 2464 pixels, pixel pitch and size 1.12 µm, Bayer filter RGGB), a reference point source and an aperture. Even though the photodetector array is a colour sensor, it behaves as a monochromatic one in the near infrared at λ=785 nm, which allows us to use it at its full spatial resolution. For a compact design, the reference source *R*

needs to illuminate the whole sensitive area of the CMOS from a short distance, which means that a highly divergent beam is required. The imaging numerical aperture of the CI is given by:

$$\mathrm{NA}=n\sin\theta=\frac{nD}{\sqrt{D^2+4Z^2}}, \tag{1}$$

where n is the refractive index of the medium between the aperture and the object, D is a transverse dimension of the photodetector array and Z is the distance between this and the aperture plane. Equation (1) is used to establish Z given the required design NA~0.5.

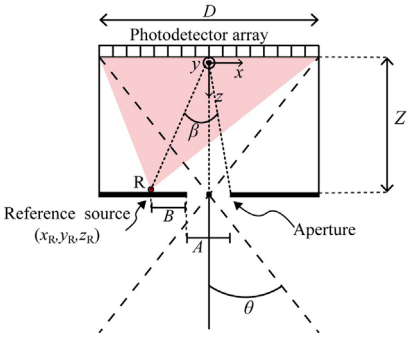

Figure 3. Coherent imager schematic diagram and its elemental components. The object usually sits some tens of cm from the aperture plane, the FOV being determined by θ.

The function of the aperture is to serve as a spatial filter so that the fringe spacing from the interference of any point in the aperture and the reference beam is larger than the Nyquist spacing d_{fA}, equal to twice the pixel pitch, to prevent aliasing of the hologram. Another function of the aperture is to control the relationship between FOV and resolution of the object reconstruction. Dimensions A, B and Z in Fig. 3 are related to the angle β between a ray from the reference source to the centre of the photodetector array and a ray from the furthest edge of the aperture to the centre of the array. β is chosen so that a hologram of the entrance pupil is band limited by the pixel separation and to separate the cross correlation terms in the frequency domain by the reference spatial carrier

$$d_{fA}<\frac{n_2\lambda}{2\sin\beta}, \tag{2}$$

where λ is the wavelength of the reference and illumination sources, and n_2 is the refractive index of the medium between the aperture and the photodetector array. In terms of A, B and Z

$$\beta=\tan^{-1}\left(\frac{A/2}{Z}\right)+\tan^{-1}\left(\frac{A/2+B}{Z}\right). \tag{3}$$

2.2. Coherent imagers

A first prototype of the CI was setup with bulk optics using a classic configuration, see Fig. (4), to assess the expected performance and to establish a methodology for data reconstruction. A reference beam with high NA was produced by focusing a laser beam with a 40× microscope objective. Light from the object and the reference beam is combined using a cube beam splitter with 5 mm sides. The CMOS sensor was cemented to one face of the cube.

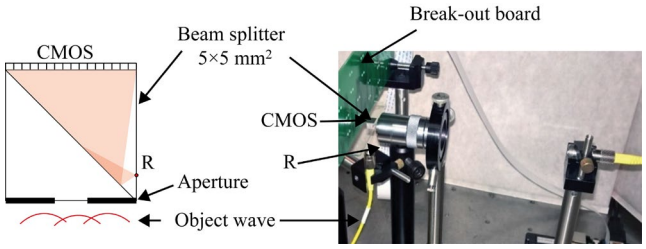

Figure 4. Coherent imager in a classic configuration using a microscope objective and a cube beam splitter.

A break-out board can be seen in Fig. (4), with electrical connectors for several CMOS sensors to form a linear array.

A second CI prototype replaces the microscope objective with graded-index (GRIN) lenses that image the output of a SM optical fibre with NA=0.12 onto a spot at the beam splitter face, so that a point source with large NA is obtained (see Fig. (5). An aperture is placed on the beam splitter's front face to band limit the holograms.

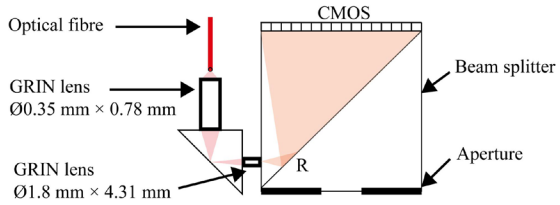

Figure 5. Coherent imager with GRIN lenses for a compact, high NA reference source.

The drawback with this approach, however, is the large number of parts and assembling costs (5 cemented optical elements + sensor), and alignment and positioning of parts can be challenging.

A third approach consists of eliminating the GRIN lenses and cementing a high-NA optical fibre directly to the side wall of the cube beam splitter. The native NA of the fibre SM600 is 0.12. This was increased by NA>0.5 by: 1) terminating the fibre with a ceramic ferrule, 2) coating the ferrule head with gold and 3) milling a small pinhole on the gold coating at the centre of the fibre core using a focused ion beam (FIB). To obtain an aberration free and spatially filtered reference beam with NA=0.5 at λ=785 nm requires a pinhole with diameter $a \sim \lambda/2NA$=785 nm (see Fig. 6).

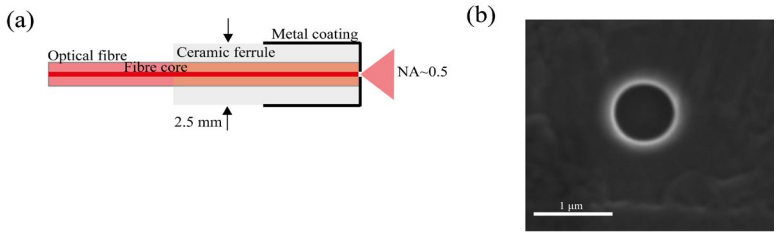

Figure 6. (a) Ferrule terminated fibre with a pinhole milled using FIB. (b) SEM image of the milled pinhole.

Figure 7 shows a CI with a high NA reference source fabricated as described above. The casing was 3D printed with ABS polymer and it accommodates the sensor with its PCB, a cube beam splitter and the ferrule with the pinhole, all fixed with optical grade potting compound[12].

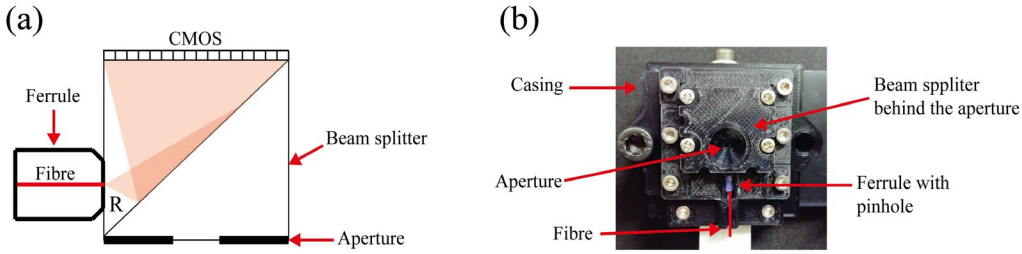

Figure 7. (a) The reference source in this CI emanates from a pinhole milled with FIB on a ferrule terminated fibre (b) 3D printed ABS working prototype of the coherent imager.

Index matching oil is used between the beam splitter and the ferrule terminated optical fibre to avoid interference fringes due to multiple reflections at the ferrule/beam splitter coupling. This prototype is compact and stable, but the beam splitter (even with NIR AR coating) introduces unwanted reflections (as in the previous prototypes) and restricts the minimum *Z*.

A fourth CI prototype eliminates the beam splitter and the ferrule. It has been demonstrated before that by replacing the cube beam splitter in a conventional digital holographic setup with a side launch reference beam leads to a compact

holographic camera design[13]. This approach, however, leads to reference wavefront aberrations and multiple optical elements are required to couple light onto a slab that guides the reference beam by total internal reflection. In our most compact CI prototype, the reference beam is launched from a bare fibre with its end polished at an angle of 90° and coated with silver. A pinhole is milled with a FIB on the fiber cladding surface so that a highly divergent beam exits the fibre with its axis perpendicular to the fibre axis (see Fig. 8).

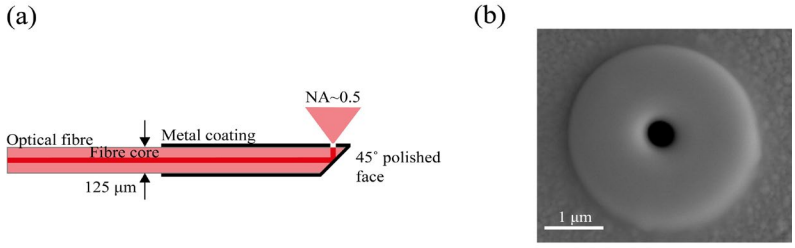

Figure 8. (a) 45° polished fibre end with high NA output. (b) SEM image of a pinhole with a diameter of 507 nm milled with FIB onto a platinum disk deposited on silver.

The grain structure of the silver coating prevents the fabrication of sub µm diameter pinholes with uniform transmission and sharp edges. This is solved by depositing a platinum disk on top of the silver, which leads to high quality pinholes with sub µm diameters -see Fig. 8(b). This fabrication process results in a very compact launch of the reference beam with a high NA as required to illuminate the whole sensor from a short standoff distance. This bare optical fibre with a lateral pinhole at the tip substitutes both the beam splitter and the ferrule in the previous prototype, having as a result a CI that is more compact and easier to assemble. Figure 9 shows a CI with an imaging NA=0.56 that incorporates a Sony IMX219, 8MP CMOS sensor, a 1.25×1.25 mm^2 aperture and a 45º polished fibre with a FIB milled pinhole as the reference source. All the components are held together inside an ABS 3D printed casing.

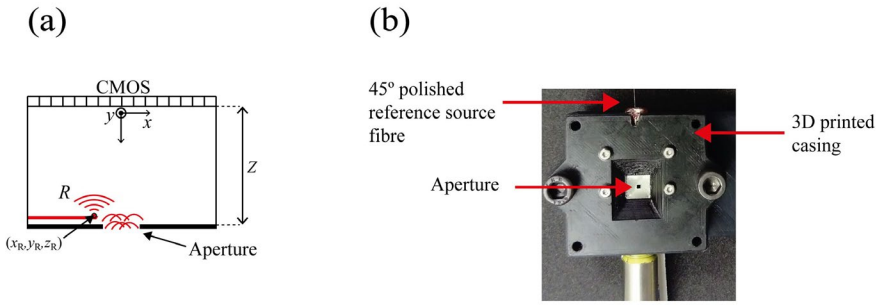

Figure 9. (a) The reference source in this CI emanates from a pinhole milled with FIB at the tip of a bare fibre -see Fig. 8(a). (b) 3D printed ABS working prototype of the coherent imager.

2.3. Hologram recording and reconstruction

Let's consider the CI illustrated in Fig. 9(a). The CMOS sensor records a hologram H

$$H = |R_s + E_s|^2 = |R_s|^2 + |E_s|^2 + R_s^* E_s + R_s E_s^*, \quad (4)$$

where R_S and E_S are the reference and aperture fields at the plane of the photodetector array, respectively, and * indicates complex conjugation. All terms are a function of position on the photodetector array and the origin of our coordinate system is at the centre pixel of the array. Our goal is to reconstruct the field at the object. In conventional off-axis Fourier holography, the reference beam introduces a space invariant carrier frequency in the Fourier transform of H. In our case, the highly divergent reference beam introduces a position dependent carrier and the hologram cannot be demodulated by a simple Fourier transform and filtering approach. However, if the reference field R_S is known, the hologram demodulation can be done as follows: first, the field at the aperture, E_A, is calculated, and then this is propagated to the object.

The term $|R_s|^2$ can be measured directly by recording the reference wavefront intensity (object illumination turned off) and then subtracted from H leaving

$$H - |R_s|^2 \approx R_s^* E_s + R_s E_s^* . \quad (5)$$

The term due to the aperture field, $|E_s|^2$, can be neglected if the reference beam intensity is much higher than the object beam passing through the aperture ($|R_s|^2 >> |E_s|^2$) [5]. The next step in the demodulation process is to divide the terms in Eq. (4) by the conjugate of the reference wave R_s^* which leads to

$$H_{dem} \approx E_s + \frac{R_s}{R_s^*} E_s^* \quad (6)$$

The first term is the field from the object that went through the aperture and reached the sensor. The second term is its conjugate times the phase term R_S/R_S^*. By propagating H_{dem} a distance Z from the sensor plane to the aperture, e.g. using angular spectrum propagation (ASP), the field E_A at the aperture is obtained, separated from the second term in eq. (5) by the angular subtense between the reference source and the centre of the aperture[12]. E_A is finally isolated at the aperture plane by masking out the other terms and propagated to the object for the final reconstruction, e.g. if the object to aperture distance is known, by adding a phase focusing term in the frequency domain.

3. REFERENCE SOURCE CHARACTERIZATION

The demodulation and reconstruction process described above requires a precise knowledge of the reference field at the sensor, which for a point source can be determined from the source position relative to the sensor, and the wavelength. A point source at coordinates (x_R, y_R, z_R) (pinhole at the end of the reference fibre) determines a complex field at the sensor

$$R(x,y) = A_0 \exp\left[-j \frac{2\pi}{\lambda} |\vec{r}(x,y,z)| + \varphi_0 \right], \quad (7)$$

where $A_0(x,y)$ is the amplitude, $\vec{r}$ is the position vector with $|\vec{r}| = \sqrt{(x-x_R)^2 + (y-y_R)^2 + z_R^2}$ the distance from the source to a pixel at (x,y,z) and φ_0 is a phase offset that is determined by calibration. The source position (x_R, y_R, z_R) is found via optimization, on the hypothesis that there is a unique position (x_R, y_R, z_R) for which plane waves arriving at the aperture from any set of arbitrary directions can be reconstructed simultaneously as point sources at infinity. A set of 11×11 plane waves with different propagation directions was generated using a Dammann grating illuminated by a plane wave in front of the CI aperture, as illustrated in Fig. 10. A hologram of the grating diffracted orders is then recorded and processed following the methodology described above.

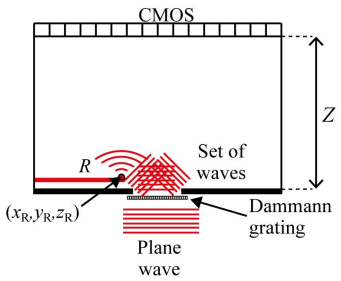

Figure 10. Reference source characterization setup.

The position of the pinhole is found iteratively: the diffracted orders of the grating are first reconstructed with an initial guess of (x_R, y_R, z_R) =(-0.083 µm,0.050 µm,3.591 mm), which results in defocused versions of point sources at infinity - see Fig. 11(a). A 2D Gaussian peak is fitted to each point source reconstruction (effectively to the central lobe of the 2D sinc function that is the Fourier transform of the square aperture) and a cost function Q is evaluated as

$$Q = \sum_{m=1}^{M} \frac{\sigma_m}{I_m} \quad (8)$$

where I and σ are the amplitude and standard deviation of a 2D Gaussian function fitted on each reconstructed diffraction order m and M=121. The pinhole position is found by searching for the reference source coordinates that minimize Q. This corresponds to reconstructed point sources at infinity that are all simultaneously in focus (narrow standard deviation σ) with maximum amplitude I. The main concept behind this approach is that only one reference wave, i.e. the source at

the correct position, can produce a stigmatic image of all the reconstructed point sources at infinity over the whole field of view of the sensor. Due to the presence of multiple local minima in Q, the minimization was performed in two stages. First a low-resolution search is performed where the position of the reference source is varied in the 3 directions x, y and z by an amount of 10 μm within a cube of 210 μm^3 centered on an initial guess reference position. Within that volume of the cost function values, a minimum is found with its respective reference source position. Subsequently, a high-resolution minimization is performed around that minimum point but now the exploring steps on the reference source position are each 0.5 μm on each axis within a cube of 15 μm^3 centered at the previous low-resolution minimum. Finally, a minimum is found to within ~ λ/4 on the high-resolution search giving as a result the position of the reference beam (x_R, y_R, z_R)=(-0.086 μm,0.048 μm,3.589 mm). Figure 11(b) shows the reconstruction after finding the reference source position by cost function minimization.

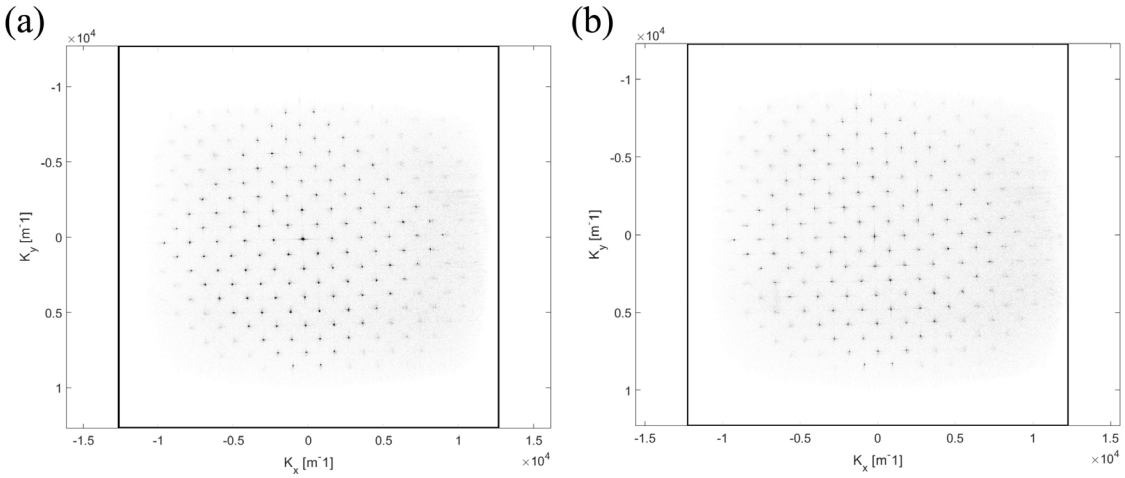

Figure 11. (a) Reconstruction (in reverse contrast) of the Dammann grating diffraction orders using an initial guess reference source position to demodulate the hologram. (b) Sharper reconstruction of the Dammann grating diffraction orders using the optimized reference position.

4. EXPERIMENT AND RESULTS

To validate the performance of the CI and evaluate its NA, a 51 mm × 76 mm aluminium test plate, see Fig. 12(a), was placed 80 mm away from the aperture. Furthermore, a laser diode (LP785-SAV50, λ=785 nm) is used to provide the illumination and reference beams. The hologram was recorded and demodulated using the position of the reference source as obtained from the optimization approach. The demodulated field was then back propagated to the aperture using ASP to obtain the field at the aperture. Finally, the unwanted terms at the aperture plane were masked out and the field at the aperture was propagated to the object plane. The reconstruction of the object is shown in Fig. 12(a).

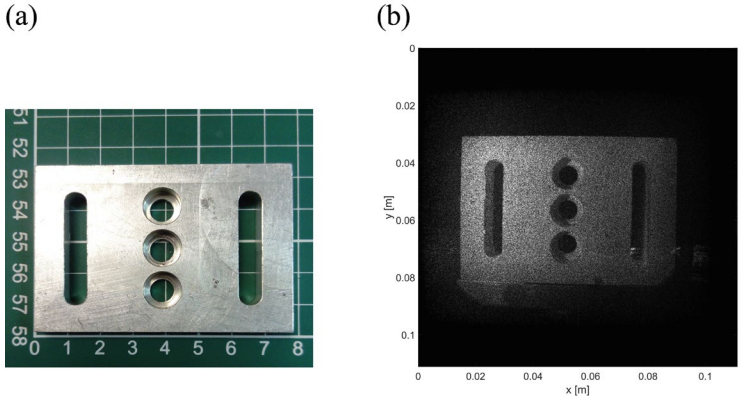

Figure 12. (a) Test plate used to demonstrate the high NA performance of the CI (Grid: 1 cm/div); (b) Holographic reconstruction.

It can be seen from Fig. 12(b) that the size of the FOV is ~110 mm in the *x* axis. The object was placed 80 mm away from the aperture of the CI, which corresponds to an imaging NA~0.56.

5. CONCLUSIONS

We presented the design of various prototypes of coherent imagers with the purpose of assembling an array of them for SAI reconstructions of large fields of view with high resolution. A compact solution was found by introducing a reference beam as a point source close to the CMOS sensor using a pinhole milled at the tip of a fibre using a focused ion beam. This approach would allow the construction of CIs as small as ~10 mm ×10 mm ×10 mm including the casing, to achieve a tight packing of coherent imagers in the array. Additionally, an optimization approach is presented to find the position of the reference source to demodulate the holograms taken with the CI and reconstruct the object or surface under study. The reconstruction of a large object close to the aperture, confirmed a large field of view that corresponds to an imaging NA~0.56.

The size of the CI can be reduced even further by using just the CMOS sensor on a smaller casing connected to a break-out board. This suggests that several CIs could be arranged with an inter-apertures distance of ~12.5mm, limited only by the electrical connectors of the CMOS cameras. By using multiple wavelengths an array of Cis can be used for surface profilometry of large areas at high spatial resolution.

6. ACKNOWLEDGMENTS

We are grateful to Epigem Ltd, the National Physical Laboratory, the CDT-EI and the EPSRC for their support of this and closely related work.

REFERENCES

[1] Leach, L., [Optical measurements of surface topography], Springer-Verlag Berlin Heidelberg, chap. 1 (2011).
[2] Garcia-Sucerquia, J., Xu, W., Jericho, S. K., Klages, P., Jericho, M. H. and Kreuzer, H. J., "Digital in-line holographic microscopic", Appl. Opt., 45(5), 836-850 (2006)
[3] Wagner, C., Osten, W. and Seebacher, S., "Direct shape measurement by digital wavefront reconstruction and multi-wavelength contouring", Opt. Eng., 39(1), 79-85 (2000).
[4] Ibrahim, D. G. A. and Yasui, T., "High-precision 3D surface topography measurement using high-stable multi-wavelength digital holography referenced by an optical frequency comb", Opt. Let., 43(8), 1758-1761 (2018).
[5] Goodman, J. W., [Introduction to Fourier optics], Roberts & company, Colorado, 231-232 (2005).
[6] Fitch, J. P., [Synthetic Aperture Radar], Springer-Verlag, New York (1988).
[7] The event horizont telescope collaboration et al., "First M87 event horizon telescope results. IV. Imaging the central supermassive black hole", Astrophys. J. Lett., 875:L4, 52 pp (2019).
[8] Feng, P., Wen, X. and Lu, R., "Long working distance synthetic aperture Fresnel off-axis digital holography", Opt. Exp., 17(7), 5473-5480 (2009).
[9] Le Clerc, F. and Gross, M., "Synthetic-aperture experiment in the visible with on-axis digital heterodyne holography", Opt. Let., 26(20), 1550-1552 (2001).
[10] Binet, R., Colineau, J. and Lehureau, J., "Short-range synthetic aperture imaging at 633 nm by digital holography", Appl. Opt., 41(23), 4775-4782 (2002).
[11] Thurman, S. T. and A. Bratcher, "Multiplexed synthetic-aperture digital holography", App. Opt., 54(3), 559-568 (2015).
[12] Park, I. S., Middleton, R. J. C., Coggrave, C. R., Ruiz, P. D. and Coupland, J. M., "Characterization of the reference wave in a compact digital holographic camera", App. Opt., 57(1), A235-A241(2018).
[13] Hahn, J., Marks, D. L., Choi, K., Lim, S. and Brady, D. J., "Thin holographic camera with integrated reference distribution", Appl. Opt., 50(24), 4848-4854 (2011).